RSC Advances

PAPER

View Article Online
View Journal | View Issue

Cite this: *RSC Adv.*, 2019, **9**, 30216

Novel one pot synthesis and spectroscopic characterization of a folate-Mn_3O_4 nanohybrid for potential photodynamic therapeutic application†

Susmita Mondal,[a] Aniruddha Adhikari,[a] Monojit Das,[b] Soumendra Darbar,[c] Ahmed Alharbi,[d] Saleh A. Ahmed,[d] Siddhartha Sankar Bhattacharya,[b] Debasish Pal[b] and Samir Kumar Pal*[ab]

Received 28th August 2019
Accepted 16th September 2019

DOI: 10.1039/c9ra06835j

rsc.li/rsc-advances

Treatment of cancer using nanoparticles made of inorganic and metallic compounds has been increasingly used, owing to their novel intrinsic physical properties and their potential to interact with specific cellular sites, thereby significantly reducing severe secondary effects. In this study, we report a facile strategy for synthesis of folate capped Mn_3O_4 nanoparticles (FA-Mn_3O_4 NPs) with high colloidal stability in aqueous media using a hydrothermal method for potential application in photodynamic therapy (PDT) of cancer. The capping of FA to Mn_3O_4 NPs was confirmed using various spectroscopic techniques. In adenocarcinomic human alveolar basal epithelial cells (A549), the nanohybrid synthesised with a combination of FA and Mn_3O_4 shows remarkable PDT activity *via* intracellular ROS generation (singlet oxygen). As established by a DNA fragmentation assay and fluorescence studies, the nanohybrid can cause significant nuclear DNA damage by light induced enhanced ROS generation. In the assessment of Bax, Bcl2 provides strong evidence of apoptotic cellular death. Cumulatively, the outcomes of this study suggest that these newly synthesized FA-Mn_3O_4 NPs can specifically destroy cells with overexpressed folate receptors, thereby providing a solution in the journey of cancer eradication.

Introduction

Cancer has become one of the major threats to life expectancy of the global population during the last few decades. According to the Global Cancer Observatory (GLOBOCAN) database and World Health Organization (WHO), approximately 9.6 million deaths occurred from cancer in 2017,[1,2] among which lung cancer caused the highest rate of mortality compared to other cancer types. The available curatives for cancer *e.g.*, chemotherapy, immunotherapies and surgeries are painful, troublesome and extremely costly. Besides the high cost and side effects, the available curatives have failed to reduce the mortality rate due to cancer, hence, new alternative treatment strategies are extremely necessary.

From its discovery (by Dougherty *et al.* in 1960) the photodynamic therapy (PDT) is gradually becoming an efficacious alternative.[3] PDT requires minimal invasion for complete destruction of malignant cells, and has less side effects. In most of the cases PDT activates the ROS mediated apoptosis pathway in cancer cells that results in the annihilation of carcinoma.[4] PDT involves administration of photosensitizing agent, which may require some modulation after internalisation in specific cells followed by activation of the agent by radiation of a specific wavelength. As a result, some irreversible photo induced damage takes place in targeted cell.[3] Although, proved effective, several limitations (*i.e.*, poor water solubility, aggregate formation, high dermal toxicity and low clearance)[5,6] of the conventional organic PDT agents hinder widespread application of it in the clinical settings. In recent studies, inorganic nanoparticles emerged as an effective alternative because of its biocompatibility, high retention time in circulation, target specificity (by attaching ligand) and low toxicity.[7–9] Another problem that confines the use of PDT is the absence of a mechanism that can ensure target specific delivery (sometimes the normal cells become as vulnerable as cancer cells). In this regard, folic acid (FA) could be used as an inexpensive and stable ligand for targeting folate receptors (FR), a tumour-associated protein over-expressed in cancer cells having high binding affinity towards folic acid ($K_d \approx 10^{-10}$ M).[10] The strategy of targeting cancer cells through FRs is a well-recognized strategy due to overexpression of FR in a variety of cancer cells including those in breast, kidney, colon, ovaries, cervix and renal cell carcinomas.[10]

[a]*Department of Chemical, Biological and Macromolecular Sciences, S. N. Bose National Centre for Basic Sciences, Block JD, Sector 3, Salt Lake, Kolkata-700106, India. E-mail: skpal@bose.res.in; Fax: +91 33 2335 3477; Tel: +91 33 2335 5706/08*

[b]*Department of Zoology, Uluberia College, University of Calcutta, Uluberia, Howrah-711315, India*

[c]*Research and Development Division, Dey's Medical Stores (Mfg.) Ltd, 62, Bondel Road, Ballygunge, Kolkata-700019, India*

[d]*Department of Chemistry, Faculty of Applied Sciences, Umm Al-Qura University, 21955 Makkah, Saudi Arabia*

† Electronic supplementary information (ESI) available. See DOI: 10.1039/c9ra06835j

Recent advances in nanotherapy have created scopes of specific targeting strategies for increasing drug concentrations within tumours while restricting the undesired toxicity to its surrounding healthy cells.[11–14] Some of the nanoparticles are photosensitive agent *i.e.* those are only active in presence of specific wavelength of light. By tagging folate with photosensitized nanoparticle precise treatment of cancer *via* PDT is possible. But synthesis of folic acid capped nanomaterial is a multistep and complicated process. Previously, for synthesis of folic acid capped NPs for biomedical application, various approaches have been utilised, such as use of different organic linkers like 2,3-dibromopropionyl chloride (DBPC), *N*-hydroxysuccinimide (NHS), 1-ethyl-3-(3-dimethylaminopropyl)-carbodiimide (EDC), polyethylene glycol and polylactic-coglycolic acid based attachment.[15–20] However, the use of organic linkers to functionalize nanoparticles can increase production cost as well as can reduce the efficacy of the nanosystem. So, an alternative facile strategy is extremely needed.

Recently, many studies have used folic acid on nanocarriers for the specific targeting of over-expressing FRs on cancer cells, but information on the capping of folic acid to manganese oxide nanoparticles (Mn_3O_4 NPs) and exploration of its toxic effect have not yet been reported. In the recent years, manganese oxide nanoparticle showed promising results in the field of nanotherapy. By modulating the surface functionalization of this nanoparticle one can modulate its physicochemical, magnetic and optical properties.[21] Its ROS generation ability with different capping ligands[21–23] makes it a potential agent against cancer and associated disorders. In this study we demonstrate a one-step method for the preparation of folic acid-functionalised manganese oxide nanoparticles (FA-Mn_3O_4 NPs) which have enhanced uptake and toxicity in cancer cells upon blue light irradiation.

Material and methods

Reagents

Manganese chloride tetrahydrate, 4′,6-diamidino-2-phenylindole (DAPI), ethanol amine (EA), folic acid (FA), 2′,7′-dichlorofluorescindiacetate (DCFH-DA) and ethidium bromide (EtBr) were obtained from Sigma Aldrich (St Louis, MO, USA). We bought A549 (adenocarcinomic human alveolar basal epithelial cells) cell line from National Centre for Cell Science (NCCS, Pune, India). 3-(4,5-Dimethylthiazol-2-yl)-2,5-diphenyltetrazolium bromide (MTT) and Dulbecco's Modified Eagle's Medium (DMEM), were obtained from Hi-Media (Mumbai, India). Penicillin/streptomycin/neomycin (PSN) antibiotic, trypsin and fetal bovine serum (FBS), were procured from Gibco-Life Technologies (Gaithersburg, MD, USA). Antibodies were purchased from Santa Cruz Biotechnology, Inc. (USA). We used Millipore water whenever required. All other chemicals were purchased from Sigma Aldrich (St Louis, MO, USA) unless otherwise stated.

Synthesis of folate capped Mn_3O_4 (FA-Mn_3O_4)

Firstly, 207 g of $MnCl_2 \cdot 4H_2O$ was dissolved in 5 mL of ethanol amine and continuously stirred for 30 minutes (solution I). In the intervening period 27.5 g of folic acid (12.5 mM, pH 8) was dissolved into 5 mL of Milli-Q water (solution II). Then solution II was added dropwise to the solution I. The mixture was then again stirred for 30 minutes. After that required amount of NaOH (0.1 M) was added to the mixture to maintain the solution pH at 7. Then the whole mixture was moved into a Teflon-lined stainless-steel autoclave. It was then kept in a sealed condition at 150 °C for 18 hours. After 18 hours the mixture was permitted to cool down to normal temperature. Then we isolated the product with the help of centrifugation. Washing was carried out for four times first with water and ethanol subsequently. The resultant product then dehydrated on water bath until dark orange power was formed.

Characterization tools and techniques

High resolution TEM (HRTEM) and transmission electron microscopy (TEM) images were acquired using an FEI TecnaiTF-20 field emission HRTEM operating at 200 kV. We had prepared the sample by drop casting of NP solution on 300-mesh amorphous carbon-coated copper grid and kept it for overnight to dry at room temperature. The X-ray diffraction (XRD) patterns of the samples were obtained using a PANalytical XPERTPRO diffractometer equipped with Cu Kα radiation (at 40 mA and 40 kV) by using a scanning rate of 0.021 s^{-1} in the 2θ range from 201 to 801. Absorbance of the folate capped nanoparticle was measured by dispersing the nanoparticle in DMSO–water mixture in Shimadzu UV-Vis 2600 spectrometer. Fluorescence emission and excitation spectra of the nanoparticle were recorded using Fluorolog, Model LFI-3751 (Horiba-Jobin Yvon, Edison, NJ) spectrofluorimeter. Colloidal stability of nanoparticle was also accessed by using Shimadzu UV-Vis 2600 spectrometer.

Measurement of photo-induced ROS using DCFH

In vitro ROS generation ability of the NPs were evaluated using DCFH-DA following a reported method without any modification.[22] In short, DCFH was prepared by the de-esterification reaction of DCFHDA at room temperature. At first, we mixed 0.5 mL of 1.0 mM DCFH-DA in methanol in presence of 2.0 mL of 0.01 N NaOH for 30 min at room temperature. The resultant mixture was neutralized with 10 mL of 25 mM NaH_2PO_4 at pH 7.4. The resultant solution was kept at 4 °C in the dark until use. To this solution NPs were added and ROS generation capacity was accessed through monitoring of fluorescence emission at 520 nm upon excitation at 488 nm. ROS generation ability at different wavelength of light irradiation after adding the nanoparticle (dispersed in DMSO, water mixture) into reaction media containing DCFH was measured and the change in fluorescence was reported.

Cytotoxicity test for A549 lung cancer cell

A549 cells were cultured at 37 °C in a humidified atmosphere under CO_2 (5%) in DMEM supplemented with 10% FBS and 1% antibiotic (PSN). After achieving 75–80% confluence, cells were harvested in phosphate buffered saline (PBS) with 0.52 mM EDTA and 0.25% trypsin. To determine the cell viability MTT assay was performed. During the initial screening, A549 cells

were incubated with FA, FA-Mn_3O_4 NPs, and DMSO–water mixture for 6 hours. After 6 hours of incubation, we rinsed the cells with PBS. Then MTT solution was added to each well and kept for 4 h in an incubator to form formazan salt. In the next step DMSO was used to solubilize the formazan salt and the absorbance was recorded using an ELISA reader (BioTek Instruments, Inc., Vermont, USA) at 595 nm.[15] Cell viability was determined as follows:

$$\text{Cell viability} \quad (\%) = \frac{\text{Abs}_{\text{control}} - \text{Abs}_{\text{sample}}}{\text{Abs}_{\text{control}}} \times 100$$

here $\text{Abs}_{\text{sample}}$ denotes the absorbance values of treated cell and $\text{Abs}_{\text{control}}$ is denoting the same for untreated cells.

In vitro photodynamic therapy (PDT)

Based on the initial screening result, a specific concentration was choose for the *in vitro* PDT assay. A549 cells were incubated in a time-dependent manner (5, 10, 15, 20, 25 and 30 min) with 0.31 μg mL^{-1} of FA-Mn_3O_4 under blue light irradiation following the MTT assay for determination of effective dose of photodynamic therapy.

Measurement of intracellular ROS generation

Intracellular ROS production was examined using DCFH-DA, which is a well-known ROS generator. Briefly, the treated cells were incubated at 37 °C for 25 min with 10 mM of DCFH-DA. Upon excitation at 488 nm fluorescence intensity was recorded at 522 nm. The intracellular ROS was also measured using fluorescence microscopic technique (Olympus BX51 fluorescence microscope, Olympus Optical Co. Ltd, Sibuya-ku, Tokyo, Japan) and ImageJ software was used to analyse the photographs (http://rsb.info.nih.gov/ij/).

Determination of nuclear condensation and fragmentation using fluorescence microscopy

To assess chromatin condensation or nuclear damage, A549 cells were incubated with or without FA-Mn_3O_4 NPs (0.31 μg mL^{-1}) along with light exposure (15 min). Then both groups of cells were stained using DAPI (50 mg mL^{-1}) for 10 min. With a fluorescence microscope (Olympus BX51, Olympus Optical Co. Ltd, Sibuya-ku, Tokyo, Japan) the images were obtained and ImageJ software was used to analyse the images (http://rsb.info.nih.gov/ij/).

Western blotting analysis

After protein isolation, mitochondrial and cytosolic content of Bax, Bcl-2 and GAPDH were analyzed using Western blotting. In brief, 25 mM HEPES buffer, pH 7.5, containing 5 mM EDTA, 2 mM dithiothreitol, 1% CHAPS, and 1 μg mL^{-1} pepstatin, leupeptin, and aprotinin were used to homogenize tissue sample. Centrifugation of homogenates were done at 14 000*g* for 20 min at 4 °C. Then the pellet was discarded and supernatants were stored. Protein concentrations in the extracts were evaluated using the bicinchoninic acid kit (Autospan Liquid Gold, Span Diagnostics Ltd., Surat). Then western blotting analysis was done with 10 μg of proteins aliquots. The proteins were transferred electrophoretically (Trans-Blot Turbo Transfer System, Biorad Laboratories Inc., CA, USA) onto poly screen polyvinylidene difluoride (PVDF) membranes (Biorad Laboratories Inc., CA, USA) after subjected to electrophoresis on 15% polyacrylamide gels containing 0.1% SDS, 5% non-fat dried milk dissolved in Tris-buffered saline containing 0.1% Tween 20 (TBST) was used to block the membranes for 1 h at RT. After washing three times with the same, the membrane was incubated with TBST containing 5% dried milk and anti-Bcl-2, anti-Bax and anti-GAPDH monoclonal antibody (Cell Signaling Technology Inc., MA, USA) for 2 h at RT. After repeated washing with TBST, the membrane was incubated with horseradish peroxidase (HRP) conjugated anti-rabbit IgG antibody (Santa Cruz Biotechnology, CA, USA) for 1 h at RT. Protein bands were visualized by using an enhanced chemiluminescence kit and an image analyser. Optical densities of the bands were measured using ImageJ software (http://rsb.info.nih.gov/ij/) and normalized against GAPDH.

Determination of DNA fragmentation using agarose gel electrophoresis

Total hepatic DNA was isolated following a standard procedure described earlier.[24] Aliquots of DNA solution were prepared and stored at 4 °C. From absorption at 260 nm DNA concentration was assessed. Hepatic DNA (5.0 μg) stained with ethidium bromide was loaded on 1.5% agarose gels for observing the DNA fragmentation. We performed electrophoresis for 2 h at 90 V, and gels were photographed under UV transillumination (InGenius3 gel documentation system, Syngene, MD, USA).

Statistical analysis

Mean ± standard deviation (SD) was used to express quantitative data unless otherwise specified. To compare different parameters between the groups we used a computer program GraphPad Prism (version 5.00 for Windows), GraphPad Software, California, USA. $p < 0.05$ was considered significant.

Result and discussion

Functionalization of manganese oxide nanoparticles with organic ligands like folate can significantly alter their surface electronic structures.[21] So, at first we have observed the UV-vis electronic absorption pattern of as prepared Mn_3O_4 NPs (thin film on quartz plate) (ESI Fig. S1†), folic acid and FA-Mn_3O_4 NPs (~pH 7.0). The as prepared Mn_3O_4 NPs exhibited no distinct signature in the UV-visible region. Folic acid has displayed characteristic absorption pattern with peaks 260 nm and 340 nm (Fig. 1a) which can be attributed to π–π* (for both alkyl and aromatic group) and n–π* (due to presence of COOH, –NH, NH_2 and C=O groups) intraligand transitions.[25] In the case of FA-Mn_3O_4 NPs, the characteristic absorption pattern of the folic acid disappeared (shifted by ~40 nm and ~20 nm). Instead, it shows one high energy peak at 300 nm and a shoulder around 360 nm (Fig. 1a), along with a low energy peak at 410 nm (Fig. 1a-inset). The peak at 300 nm could be possibly due to

ligand-to metal charge transfer (LMCT) processes involving folate–$Mn^{3+/4+}$ interaction, one of the high energy charge transfer process.[21,26] The other expected LMCT band at around 385 nm has not been appeared in the absorption spectrum presumably because of the more intense absorption at 300 nm that has obscured it. However the band at 385 nm is distinctly visible in the excitation spectrum at around 385 nm (Fig. 1b). The other band at 410 nm is reasonably attributed to d–d transitions of Mn^{3+} in FA-Mn_3O_4 NPs, as the degeneracy of ^5E_g ground state term of d^4 (Mn^{3+}) high-spin octahedral environment, has been lifted by the Jahn–Teller effect, that ultimately leads to a tentative assignment of the observed band to the transitions $^5B_{1g} \rightarrow {}^5E_g$. The other possible low energy transitions *e.g.*, $^5B_{1g} \rightarrow {}^5B_{2g}$, and $^5B_{1g} \rightarrow {}^5A_{1g}$ are not evident because previous studies have shown this transition happens in presence of ligands with alpha hydroxy carboxylate groups. In summary, the absorbance studies confirms the functionalization of the NPs with folate. Fluorescence emission spectrum upon excitation at 280 nm for FA and FA-Mn_3O_4 NP (Fig. 1b) gave a precise insight of the nanohybrid. The relatively low quantum yield emission peak of FA at 340 nm arises from *p*-aminobenzoyl-L-glutamic acid.[21,26,27] Upon functionalization, this 340 nm peak becomes prominent along with significant quenching of the emission peak of FA at 460 nm which originates from 6-formyl pterin residue.[28] These changes in characteristic peaks of folic acid provide essential information about attachment of folic acid with Mn_3O_4 nanoparticle. From the change in emission peak at 460 nm we can conclude that the Mn_3O_4 is attached with FA *via* 6-formyl pterin residue as electrons density responsible for this peak has shifted to nanoparticle. The emission peak at 340 nm which is present in both species help us to prove the presence of *p*-aminobenzoyl-L-glutamic residue of FA in the synthesized nanomaterial. Hence from absorbance and fluorescence spectra we can conclude that the FA has successfully capped with the Mn_3O_4 nanoparticle.

A transmission electron microscopy (TEM) study has been performed to characterize the water soluble FA-Mn_3O_4 NPs in detail and also to confirm the functionalization process. As illustrated in Fig. 2a, TEM analysis revealed the spherical shape of the FA-Mn_3O_4 NPs with average diameter of around 4.86 ± 0.24 nm (Fig. 2b). Corresponding high resolution TEM (HRTEM) image (Fig. 2c) of single particle confirms the crystalline nature of the NPs having interplanar distance of ~3.15 Å which corresponds to the spacing between the (112) planes of Mn_3O_4 tetragonal crystal lattice.[23,29] All X-ray diffraction (XRD) peaks corresponding to (101), (112), (200), (103), (211), (004), (220), (204), (105), (312), (303), (321), (224) and (400) planes of FA-Mn_3O_4 NPs (Fig. 2d) exactly reflects the tetragonal hausmannite structure of Mn_3O_4 with a lattice constant of $a = 5.76$ Å and $c = 9.47$ Å and space group of $I4_1/amd$ described in literature (JCPDS no. 24-0734).[22,23,29] Absence of any additional peaks from other phases, indicated high purity and good crystallinity of the synthesized material. From the aforementioned findings we can conclude that the hydrothermal method was able to synthesize highly crystalline Mn_3O_4 capped with folate. In our synthesis process the first step involved the mixing of $MnCl_2$ with EA (see experimental section for more details), this mixing lead to the formation of $MnCl_2(EA)_2$ complex. After this complex was formed introduction of distilled water to the mixture through folic acid solution induced the formation of Mn_3O_4.

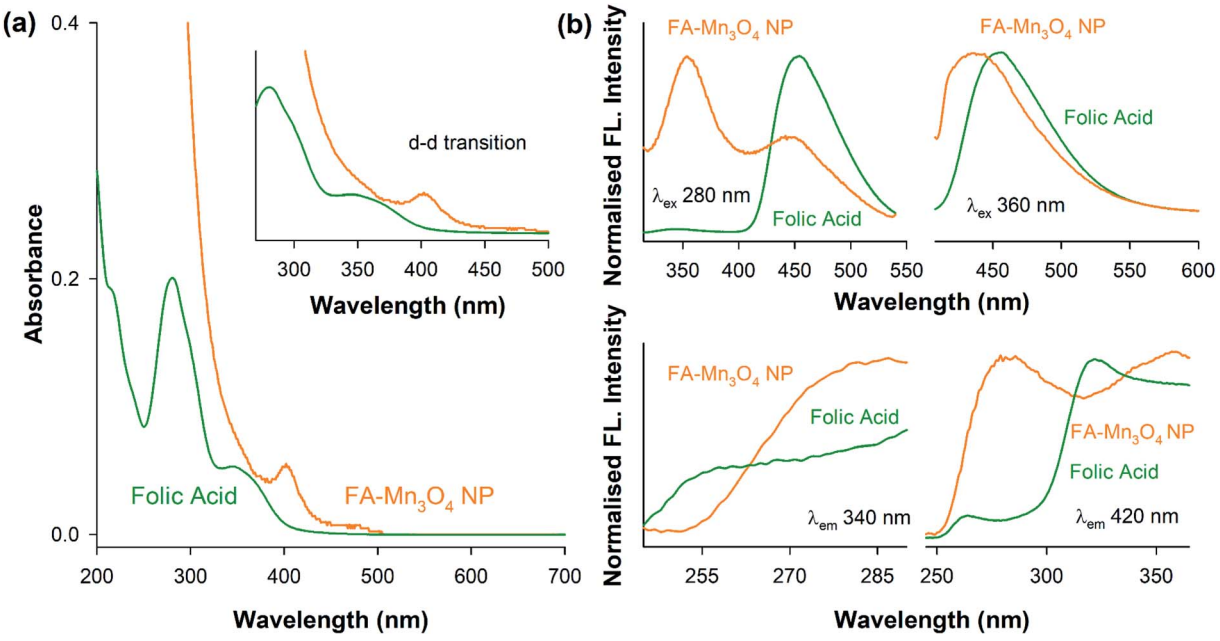

Fig. 1 Spectroscopic characterization of the nanohybrid. (a) The absorption spectra of folate-capped NPs (FA-Mn_3O_4 NPs) used as PDT agent in the present study and the capping agent folate (FA) are shown in panel. A magnified version of the absorption spectrum of the NPs in the rage of 300–500 nm is shown in the inset. The absorption peaks due to ligand to metal charge transfer (LMCT) and d–d transition (see text) are evident. (b) The corresponding emission and excitation spectra of FA and FA-Mn_3O_4 NPs.

Now the pH adjustment is required for the stability of the metal oxide. So in this process colloidal nanoparticles were formed without any additional nucleation, *i.e.* $MnCl_2$ contributed to the nucleation process whereas the growth was due to the creation of *in situ* $MnCl_2(EA)_2$ complex.[29] In the second phase the carboxy group of glutamate moiety of 6-formyl pterin residue in folic acid was attached to the nanoparticle due to higher temperature and functioned as reducing agent to decrease the size of the NPs. So, by increasing temperature we have successfully bypassed the need of organic linker to tag folic acid with nanoparticle. From the above mentioned experiments we can conclude that Mn_3O_4 has been successfully formed by hydrothermal process and capping of FA has not affected the crystal structure of the nanoparticle. The colloidal stability was also analysed for FA-Mn_3O_4 and Mn_3O_4 dispersed in DMSO–water mixture, which shows the FA capping drastically increased the solubility of the Mn_3O_4 NPs (otherwise insoluble) in aqueous media (Fig. 2e).

After detailed photophysical characterization, ROS generation ability of the nanohybrid (FA-Mn_3O_4 NP) was evaluated *in*

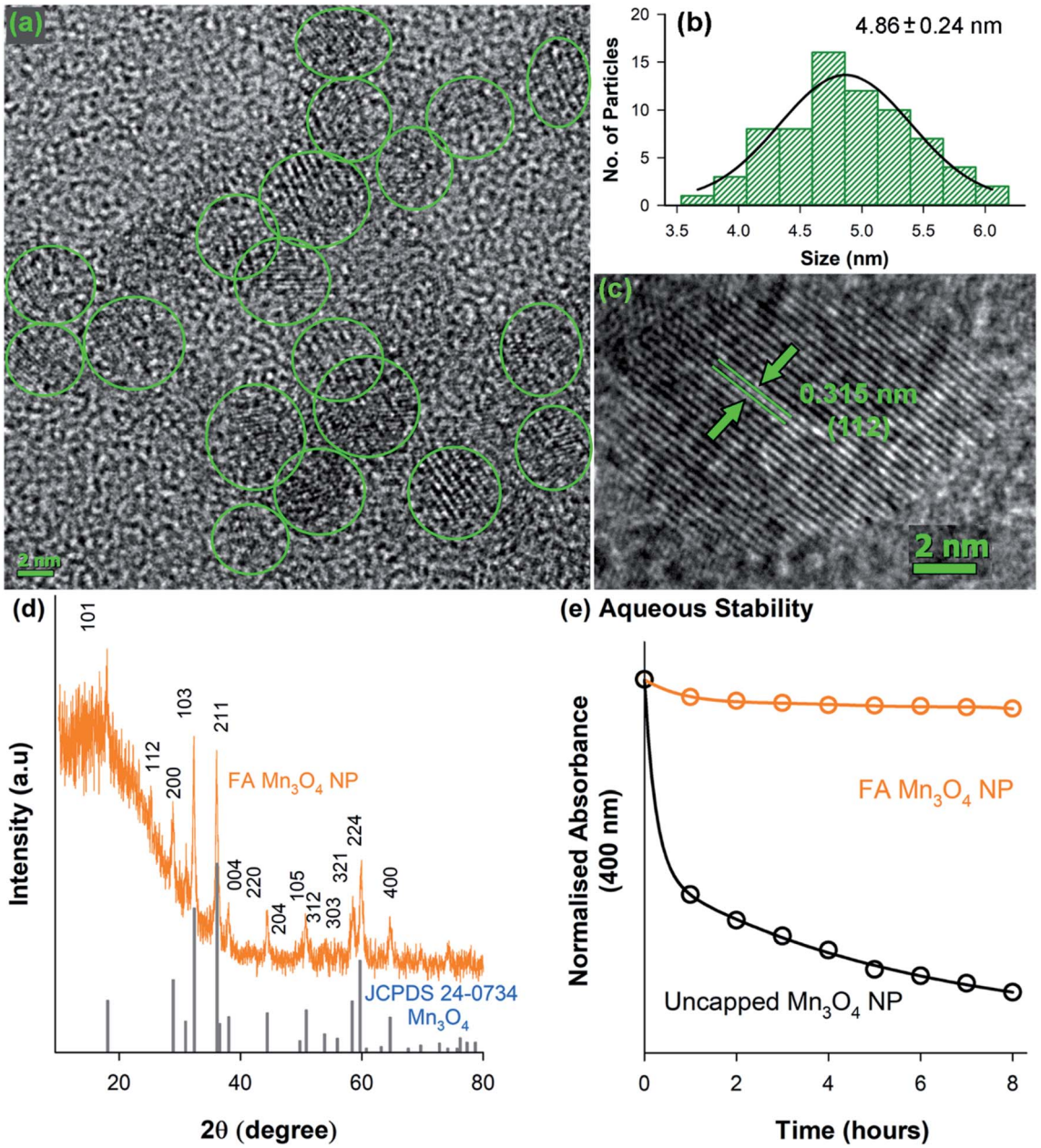

Fig. 2 Characterization of nanoparticles. (a) The particle distribution of the nanoparticles (NPs) recorded under transmission electron microscopy (TEM). (b) The particle size distribution is shown with average size of 4.86 ± 0.24 nm and (c) high-resolution electron micrograph (HRTEM) of the NPs with a clear interplanar distance of 0.315 nm for (112) planes in the Mn_3O_4 NPs is evident. (d) XRD pattern of synthesized FA-Mn_3O_4 NPs which exactly matches to that of library spectra. (e) Capping with folate increases the colloidal stability of the NPs as illustrated in time dependent absorbance studies (solid lines are guide to the eye).

vitro by monitoring the conversion of DCFH, a widely used marker for detection of ROS, to dichlorofluorescein (DCF) in aqueous medium.[30] In presence of ROS, non-fluorescent DCFH undergoes oxidation to produce florescent DCF ($\lambda_{ex} = 488$ nm; $\lambda_{em} = 520$ nm). So, we monitored the fluorescence intensity of DCF at 520 nm ($\lambda_{ex} = 488$ nm) with respect to time (Fig. 3a). FA-Mn_3O_4 NPs showed negligible ROS generation in absence of light. So, we evaluated photo induced ROS generation capability of FA-Mn_3O_4 NPs upon of a wide range of visible light irradiation (blue: 430 ± 15 nm, green: 540 ± 15 nm, and red: 640 ± 15 nm). From Fig. 3a, it is evident that the maximum increment of fluorescence intensity was obtained under blue light excitation in FA-Mn_3O_4 NPs; almost six fold increase compared to free folic acid. This enhancement in ROS generation ability in presence of blue light may be attributed to the absorption band (*i.e.*, d–d transition band) of FA-Mn_3O_4 NPs at ~410 nm, which was triggered after folic acid sensitization. Thus, exposure to the blue light facilitates the excitation followed by relocation of valence band electrons to conduction band of the metal, which in turn creates an electron–hole pair in the metal.[31–33] The excited state electrons may either migrate towards the dissolved oxygen present in the solution to reduce it to superoxide radical anion ($^{\bullet}O_2^-$), or generate singlet oxygen ($^1O_2$) during their return to the ground state.[31–33] Similarly, the holes can oxidize hydroxyl ion or water molecules and generate hydrogen peroxide (H_2O_2) or hydroxyl radical ($HO^{\bullet}$).[31–33] Although, the high amount of ROS generated due to photo-irradiation makes the nanohybrid suitable for PDT, it is important to identify the nature of ROS. However, DCFH oxidation is a non-specific marker of ROS, *i.e.*, they show similar response to superoxide

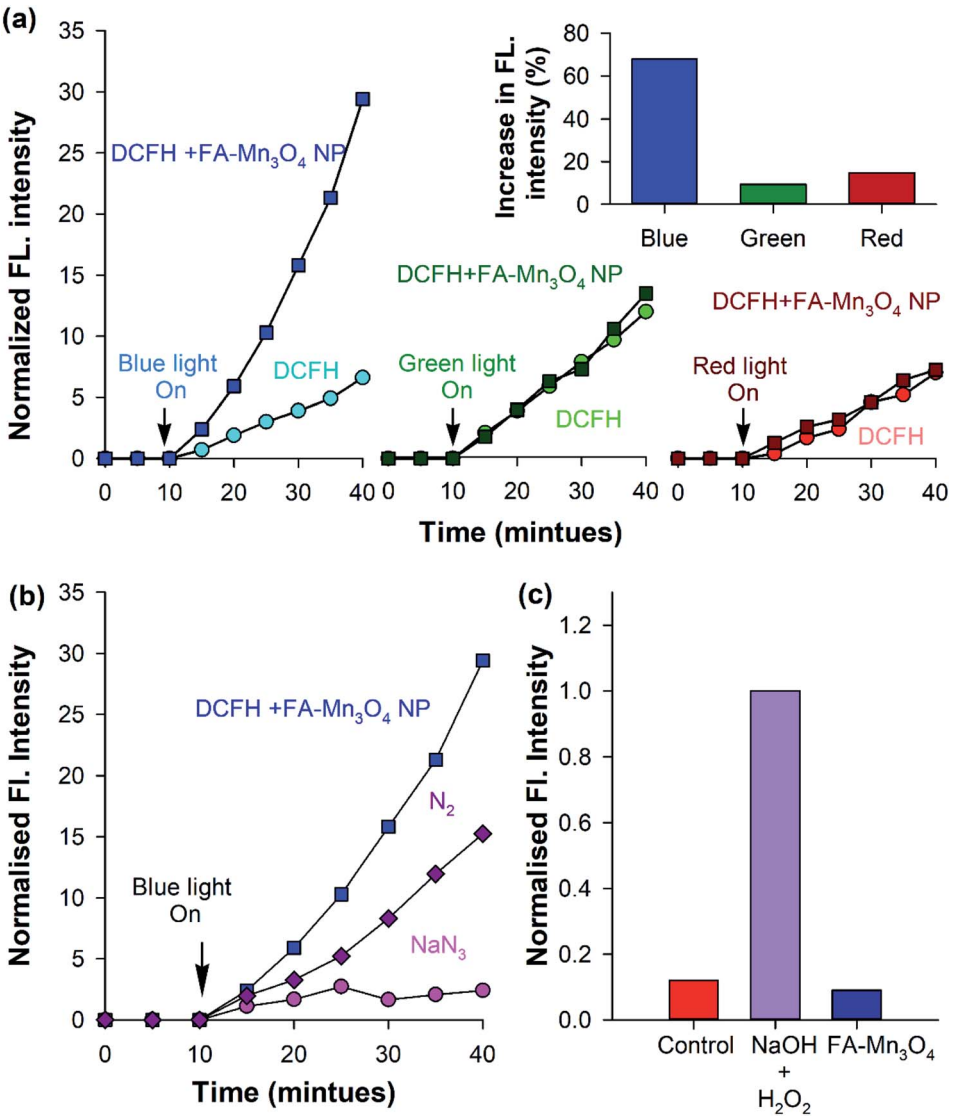

Fig. 3 *In vitro* ROS generation ability of the nanoparticles in different light illumination. (a) DCFH oxidation with respect to time in addition of FA-Mn_3O_4 NPs and control in the dark and with subsequent light (red, green and blue) irradiation. (b) DCFH oxidation with respect to time with FA-Mn_3O_4 NPs addition in an atmosphere of purged nitrogen (violet), sodium azide (pink), and a control (blue) under dark with subsequent blue-light irradiation. (c) Chemiluminescence of luminol prior to blue-light illumination for 15 min for the control, NaOH + H_2O_2 and FA-Mn_3O_4 NPs.

anions or singlet oxygen radicals. On the other hand, luminol specifically oxidizes in presence of superoxide to generate chemiluminescence.[34] As depicted in Fig. 3c, no chemiluminescence was observed in the presence of FA-Mn_3O_4 NPs after blue-light irradiation for 15 min, which rules out the likelihood of superoxide production by the nanohybrid. To investigate the participation of singlet oxygen radicals, we carried out the DCFH oxidation assay in the presence of a well-known singlet oxygen quencher, sodium azide.[23,34] The rate of DCFH oxidation (*i.e.*, increase in fluorescence intensity) was decreased significantly in presence of sodium azide (Fig. 3b). The aforementioned results clearly indicates the nature of the ROS predominantly to be singlet oxygen rather than superoxide anion, which is consistent with the previously reported mechanistic pathways of ROS generation by surface functionalized manganese oxide nanoparticles.[22,23,35] To elucidate the role of dissolved oxygen in the aforementioned ROS generation pathway, we carried out DCFH oxidation assay after nitrogen purging for one hour. The reduction in DCFH oxidation implies that the dissolved oxygen in the medium is involved in the generation of singlet oxygen.

The comprehensive characterization studies and analysis of photo-induced dynamics in FA-Mn_3O_4 NPs were followed by the use of the nanohybrid as an effective PDT agent. So, we evaluated the cytotoxicity of FA-Mn_3O_4 NPs to A549 cells (human alveolar basal epithelial cells) in both the absence and presence of 430 ± 15 nm light irradiation using MTT assay. Bioreduction of MTT leads to production of formazan,[36] which is related to mitochondrial activity (Fig. 4a) and thereby cell viability which can be estimated by measuring the absorption at 570 nm. In absence of light, the half lethal dose (LD_{50}) of FA-Mn_3O_4 NPs was found to be $\sim$2 μg mL^{-1} (Fig. 4b) at an incubation period of 6 h. For folic acid, a well-known cell nutrient, minimal cytotoxic ($\sim$5%) effect was observed at the aforementioned

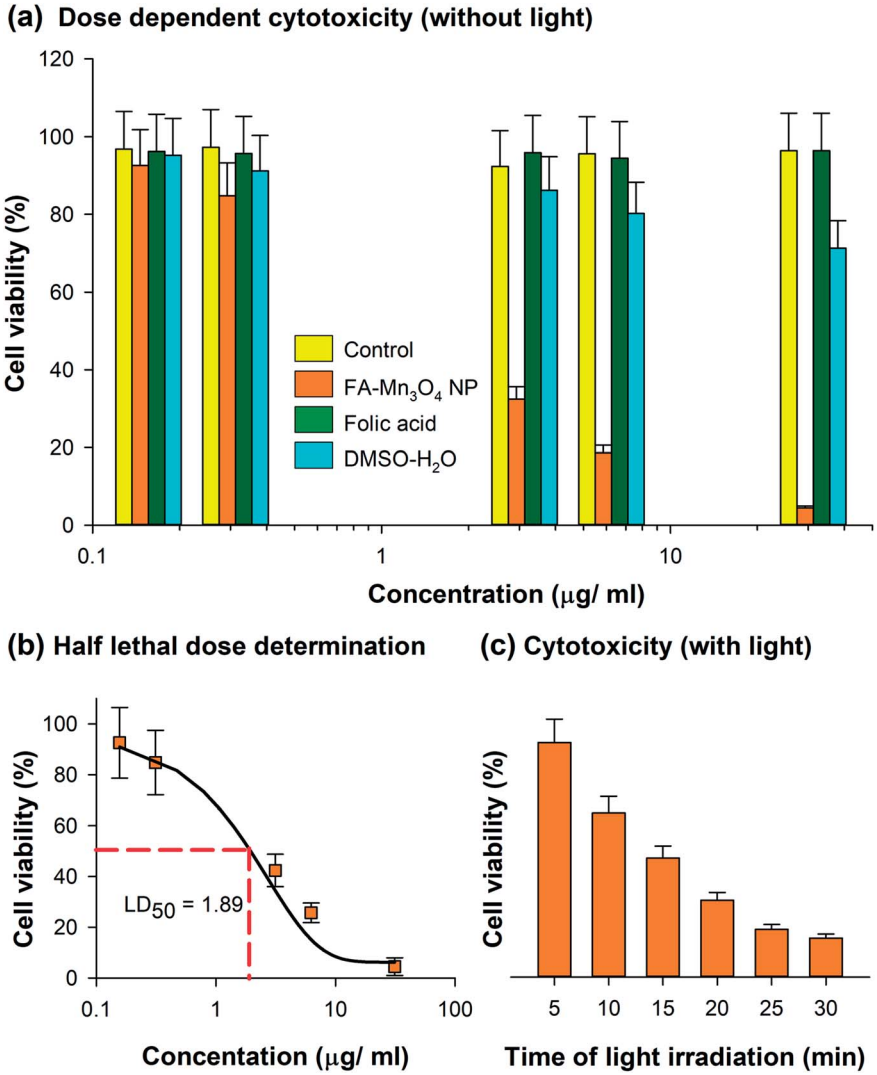

Fig. 4 Cytotoxicity of FA-Mn_3O_4 NPs in A549 cell line. (a) MTT assay quantified cell viability with different concentrations of FA, DMSO–H_2O mixture (the solvent) and FA-Mn_3O_4 NPs in the absence of blue light. (b) The LD_{50} dose found to be 1.89 μg mL^{-1} (6 h of incubation with NPs). (c) Light induced cytotoxicity after treatment with 0.31 μg mL^{-1} of FA-Mn_3O_4 NPs followed by blue light irradiation for different time durations (0–30 min).

concentration. So, we have excluded folic acid from the next part of our cellular study. For DMSO–water mixture, no significant reduction in cell viability (~15%) was found up to concentration ~2 μg mL^{-1}. As low dark and high light induced cytotoxicity are the two most essential properties of the NPs for their application in PDT,[37] we used the apparently non-toxic (cell viability ~84.8% in absence of light) concentration of 0.31 μg mL^{-1} FA-Mn_3O_4 NPs for the photo-induced cytotoxicity experiments (described in later part of the study). Next, we incubated the A549 cells with 0.31 μg mL^{-1} FA-Mn_3O_4 NPs under different time of blue light exposure. A gradual reduction in the cell viability was observed with increase in blue light irradiation time (in 5, 10, 15, 20, 25 and 30 min of light exposure cell viability was 75.5%, 52.9%, 38.4%, 24.8%, 15.4% and 12.6%, respectively) as compared to the FA-Mn_3O_4 NP treated cells without light exposure (Fig. 4c). A light dose of 20 min shows optimum effect on cell death (cell viability 24.8%) and after that the effect is minimal, suggesting a rapid ROS activity of FA-Mn_3O_4 NPs in A549 cells, consistent with extracellular ROS generation. These *in vitro* PDT experiments illustrates the photodynamic effect of FA-Mn_3O_4 NPs in destruction of lung cancer cells (A549) under blue light irradiation which may further be evaluated in animal models (which is beyond the purview of this study).

To elucidate the role of ROS in the FA-Mn_3O_4 NP-mediated PDT against cancer, the FA-Mn_3O_4 NP-loaded A549 cells were stained with DCFH-DA, an intracellular ROS probe. DCFH-DA is nonfluorescent, which is oxidized by ROS to DCF that emits at green. As depicted in Fig. 5a and b, FA-Mn_3O_4 NPs (0.31 μg mL^{-1}) showed insignificant ROS generation activity without

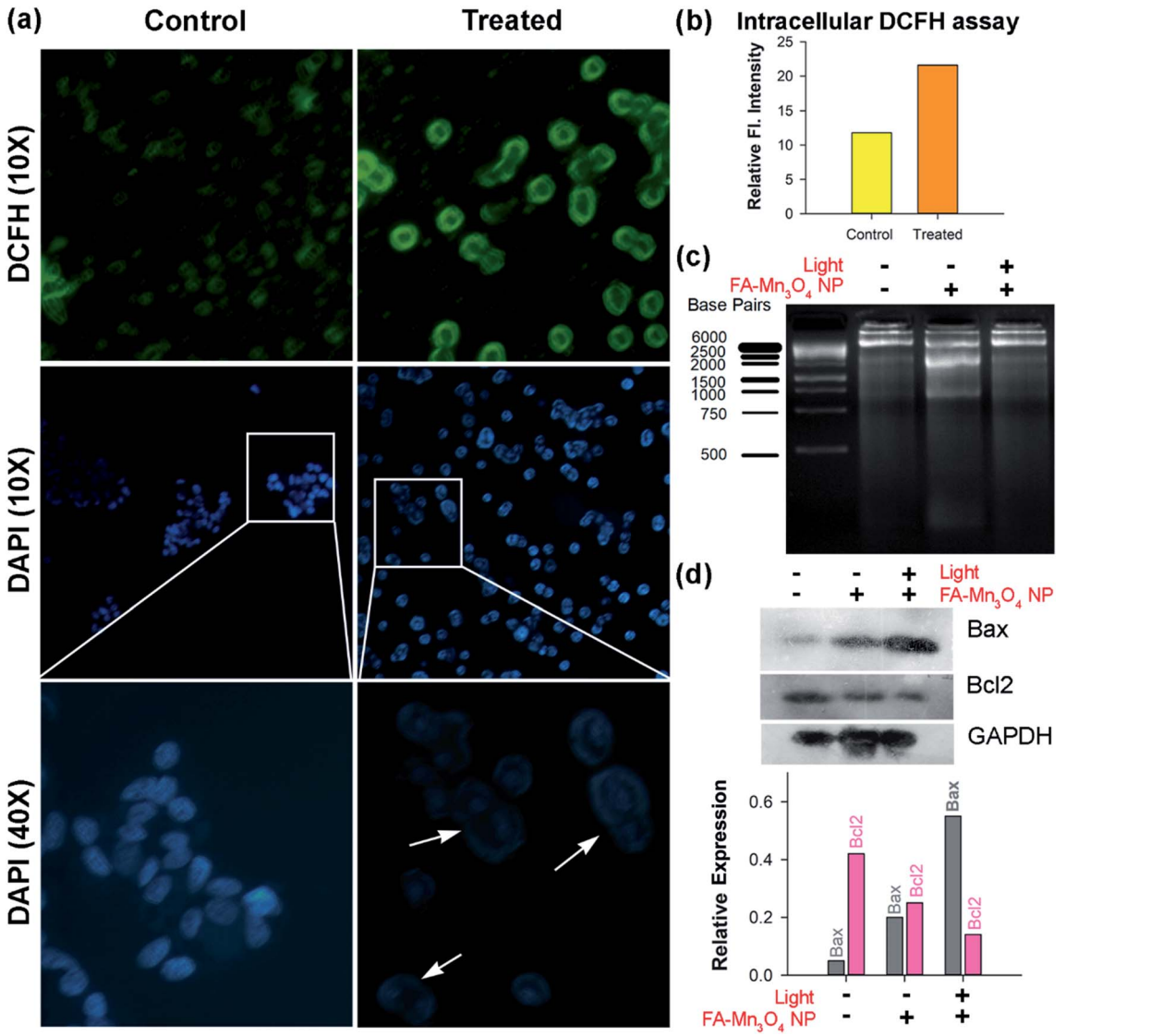

Fig. 5 Effects of FA-Mn_3O_4 NP-PDT on cancer cells *in vitro*. (a) Fluorescence microscopic images of A549 cells stained with DCFH shows increased DCF fluorescence upon photo irradiation (blue light). DAPI stained cells showed apoptotic body upon PDT using FA-Mn_3O_4 NPs. The white arrows indicate apoptotic bodies. (b) Quantification of intracellular ROS. (c) DNA fragmentation assay using gel electrophoresis technique. (d) Western blot analysis for relative change in expression levels of Bax and Bcl2 proteins, to major controller of apoptosis.

light irradiation. After irradiation with blue light for 20 min, the intracellular ROS level reached saturation, which is consistent with both extracellular ROS generation and photo-induced cytotoxicity assay. The considerable light induced enhanced intracellular ROS activity and optimum dark toxicity of 0.31 μg mL^{-1} dose of FA-Mn_3O_4 NPs indicates its potential in PDT.

Next, to understand the mode of cell death we performed microscopic studies. In bright field microscopic analysis apoptotic changes like reduction in cell size, clear cytoplasm *etc.* (morphometric data are shown in ESI Fig. S2†) become evident in case of light irradiated cells treated with FA-Mn_3O_4 NPs, whereas, the cells without light illumination showed normal morphology.[38,39] The extent of apoptosis was further evaluated using nuclear staining dye DAPI (Fig. 5a). DAPI can bind specifically to nuclear DNA and emit a blue light visible with a fluorescence microscope.[40,41] When the nuclei of A549 cells were studied by DAPI staining, we found that normal nuclei had a homogeneous pattern of staining (Fig. 5a). In contrast, FA-Mn_3O_4 NP treated (with photo irradiation) nuclei were smaller and brighter than normal cells, and nuclear fragmentation and condensation (apoptotic bodies) were evident (Fig. 5a). These findings suggest that the photo-induced FA-Mn_3O_4 NPs demonstrated changes consistent with apoptosis.[42]

The damage of nuclear DNA as observed in DAPI staining was further accessed by DNA fragmentation assay using gel electrophoresis. DNA was extracted from the nanoparticle treated cells (both in presence and in absence of blue light) and run on 1.5% agarose gel. Fig. 5c shows that in presence of blue light there was a significant damage of nuclear DNA in terms of ladder formation, a biochemical hallmark of apoptosis,[43] compared to both control and without light FA-Mn_3O_4 NP treated ones. Various studies suggest that the balance between proapoptotic (Bax/Bad) and antiapoptotic (Bcl-2/Bcl-xL) members of the Bcl-2 protein family determine the fate of a cell in physiological milieu.[40,43] Fig. 5d displays the expression of Bax which was increased in the cells that were incubated with FA-Mn_3O_4 in presence of light whereas, the expression of Bcl2 protein was drastically decreased in these group of cell. It is well know that Bcl2 protein family acts as an anti-apoptotic actor by inhibiting Bax. Thus in summary, FA-Mn_3O_4 NPs in presence of blue light increases the cellular ROS level, which triggers the Bax expression in cells. On the other hand, FA-Mn_3O_4 NPs down regulate the Bcl2 expression, in turn reduces the inhibition on Bax. As a result, increased Bax can induce the nuclear DNA fragmentation thereby dictating the cells to undergo apoptosis.

Conclusion

From this study we can conclude that we have developed a facile and cost effective method for synthesis of folic acid capped Mn_3O_4 nanoparticles without using any additional organic linker (confirmed by spectroscopic studies). This folic acid capped nanoparticle can generate ROS in presence of blue light (as depicted in both intracellular and extracellular DCFH assay) and can be used as an efficacious PDT agent against adenocarcinomic human alveolar basal epithelial cells (lung cancer cells). Nuclear DNA fragmentation, apoptotic body formation, overexpression of Bax and down regulation of Bcl2 proteins suggest the underlying mechanism to be apoptosis. Although, we have described the photo induced cytotoxicity of FA-Mn_3O_4 NPs in lung cancer cells as a model, the similar effects can be observed in other carcinomas too. Hence, blue light induced PDT can be effectively used to treat carcinomic tissues (*e.g.* lung cancer, colorectal cancer, stomach cancer, throat cancer *etc.*) by introduction of blue light using optical fibres. Finally, this work elicits a new approach towards the synthesis of effective, low cost nanohybrids for diagnosis and therapy of alveolar adenocarcinoma.

Data availability statement

The authors confirm that the data supporting the findings of this study are available within the article and/or its ESI.† Any other related data that support the findings of this study are available from the corresponding author, SKP, upon reasonable request.

Conflicts of interest

The authors confirm no conflict of interest to disclose.

Acknowledgements

SKP would like to thank Indian National Academy of Engineering (INAE) for Abdul Kalam Technology Innovation National Fellowship. The authors would like to thank DST, India, for financial grants, SB/S1/PC-011/2013. The authors also thank DBT (WB)-BOOST scheme for financial grant, 339/WBBDC/1P-2/2013.

References

1 F. Bray, J. Ferlay, I. Soerjomataram, R. L. Siegel, L. A. Torre and A. Jemal, *Ca–Cancer J. Clin.*, 2018, **68**, 394–424.
2 J. Ferlay, M. Colombet, I. Soerjomataram, C. Mathers, D. Parkin, M. Piñeros, A. Znaor and F. Bray, *Int. J. Cancer*, 2019, **144**, 1941–1953.
3 T. J. Dougherty, C. J. Gomer, B. W. Henderson, G. Jori, D. Kessel, M. Korbelik, J. Moan and Q. Peng, *JNCI, J. Natl. Cancer Inst.*, 1998, **90**, 889–905.
4 F. Yang, J. Liu, X. Jiang, W. Wu, Z. Wang, Q. Zeng and R. Lv, *RSC Adv.*, 2019, **9**, 17273–17280.
5 F. Wang, D. Banerjee, Y. Liu, X. Chen and X. Liu, *Analyst*, 2010, **135**, 1839–1854.
6 S. Zeng, H. Wang, W. Lu, Z. Yi, L. Rao, H. Liu and J. Hao, *Biomaterials*, 2014, **35**, 2934–2941.
7 R. Lv, C. Zhong, R. Li, P. Yang, F. He, S. Gai, Z. Hou, G. Yang and J. Lin, *Chem. Mater.*, 2015, **27**, 1751–1763.
8 R. Lv, P. Yang, F. He, S. Gai, G. Yang, Y. Dai, Z. Hou and J. Lin, *Biomaterials*, 2015, **63**, 115–127.
9 R. Lv, Y. Wang, J. Liu, M. Feng, F. Yang, X. Jiang and J. Tian, *ACS Biomater. Sci. Eng.*, 2019, **5**, 3100–3110.
10 C. Xing, L. Liu, H. Tang, X. Feng, Q. Yang, S. Wang and G. C. Bazan, *Adv. Funct. Mater.*, 2011, **21**, 4058–4067.

11 M. K. Yu, J. Park and S. Jon, *Theranostics*, 2012, **2**, 3.
12 H. Maeda, *Advances in enzyme regulation*, 2001.
13 T. M. Allen, *Nat. Rev. Cancer*, 2002, **2**, 750.
14 V. P. Torchilin, *Nanoparticulates as drug carriers*, Imperial College Press, 2006.
15 R. Nandi, S. Mishra, T. K. Maji, K. Manna, P. Kar, S. Banerjee, S. Dutta, S. K. Sharma, P. Lemmens, K. D. Saha and S. K. Pal, *J. Mater. Chem. B*, 2017, **5**, 3927–3939.
16 F. Sonvico, S. Mornet, S. Vasseur, C. Dubernet, D. Jaillard, J. Degrouard, J. Hoebeke, E. Duguet, P. Colombo and P. Couvreur, *Bioconjugate Chem.*, 2005, **16**, 1181–1188.
17 J.-J. Lin, J.-S. Chen, S.-J. Huang, J.-H. Ko, Y.-M. Wang, T.-L. Chen and L.-F. Wang, *Biomaterials*, 2009, **30**, 5114–5124.
18 K. Hayashi, M. Moriya, W. Sakamoto and T. Yogo, *Chem. Mater.*, 2009, **21**, 1318–1325.
19 A. J. Ditto, K. N. Shah, N. K. Robishaw, M. J. Panzner, W. J. Youngs and Y. H. Yun, *Mol. Pharm.*, 2012, **9**, 3089–3098.
20 S. Mohapatra, S. K. Mallick, T. K. Maiti, S. K. Ghosh and P. Pramanik, *Nanotechnology*, 2007, **18**, 385102.
21 A. Giri, N. Goswami, M. Pal, M. T. Z. Myint, S. Al-Harthi, A. Singha, B. Ghosh, J. Dutta and S. K. Pal, *J. Mater. Chem. C*, 2013, **1**, 1885–1895.
22 N. Polley, S. Saha, A. Adhikari, S. Banerjee, S. Darbar, S. Das and S. K. Pal, *Nanomedicine*, 2015, **10**, 2349–2363.
23 A. Adhikari, N. Polley, S. Darbar, D. Bagchi and S. K. Pal, *Future Sci. OA*, 2016, **2**, FSO146.
24 B. D. Uhal, I. Joshi, A. L. True, S. Mundle, A. Raza, A. Pardo and M. Selman, *Am. J. Physiol.: Lung Cell. Mol. Physiol.*, 1995, **269**, L819–L828.
25 M. G. A. El-Wahed, M. S. Refat and S. M. El-Megharbel, *Spectrochim. Acta, Part A*, 2008, **70**, 916–922.
26 M. E. Bodini, L. A. Willis, T. L. Riechel and D. T. Sawyer, *Inorg. Chem.*, 1976, **15**, 1538–1543.
27 Y.-F. Han, F. Chen, Z. Zhong, K. Ramesh, L. Chen and E. Widjaja, *J. Phys. Chem. B*, 2006, **110**, 24450–24456.
28 M. K. Off, A. E. Steindal, A. C. Porojnicu, A. Juzeniene, A. Vorobey, A. Johnsson and J. Moan, *J. Photochem. Photobiol., B*, 2005, **80**, 47–55.
29 S. Lei, K. Tang, Z. Fang and H. Zheng, *Cryst. Growth Des.*, 2006, **6**, 1757–1760.
30 S. Chaudhuri, S. Sardar, D. Bagchi, S. Dutta, S. Debnath, P. Saha, P. Lemmens and S. K. Pal, *ChemPhysChem*, 2016, **17**, 270–277.
31 J. Bogdan, J. Pławińska-Czarnak and J. Zarzyńska, *Nanoscale Res. Lett.*, 2017, **12**, 225.
32 I. Grčić, D. Vujević, K. Žižek and N. Koprivanac, *React. Kinet., Mech. Catal.*, 2013, **109**, 335–354.
33 A. Mills and S. Le Hunte, *J. Photochem. Photobiol., A*, 1997, **108**, 1–35.
34 S. Sardar, S. Chaudhuri, P. Kar, S. Sarkar, P. Lemmens and S. K. Pal, *Phys. Chem. Chem. Phys.*, 2015, **17**, 166–177.
35 A. Giri, N. Goswami, C. Sasmal, N. Polley, D. Majumdar, S. Sarkar, S. N. Bandyopadhyay, A. Singha and S. K. Pal, *RSC Adv.*, 2014, **4**, 5075–5079.
36 M. Ishiyama, H. Tominaga, M. Shiga, K. Sasamoto, Y. Ohkura and K. Ueno, *Biol. Pharm. Bull.*, 1996, **19**, 1518–1520.
37 J. Tian, L. Ding, H.-J. Xu, Z. Shen, H. Ju, L. Jia, L. Bao and J.-S. Yu, *J. Am. Chem. Soc.*, 2013, **135**, 18850–18858.
38 S. Elmore, *Toxicol. Pathol.*, 2007, **35**, 495–516.
39 F. Lang, E. Gulbins, I. Szabo, A. Lepple-Wienhues, S. M. Huber, C. Duranton, K. S. Lang, P. A. Lang and T. Wieder, *J. Mol. Recognit.*, 2004, **17**, 473–480.
40 F. Lian, Y. Li, M. Bhuiyan and F. H. Sarkar, *Nutr. Cancer*, 1999, **33**, 125–131.
41 Y. Teow and S. Valiyaveettil, *Nanoscale*, 2010, **2**, 2607–2613.
42 F. J. Blanco, R. Guitian, E. Vázquez-Martul, F. J. de Toro and F. Galdo, *Arthritis Rheum.*, 1998, **41**, 284–289.
43 P. B. Pal, K. Sinha and P. C. Sil, *PLoS One*, 2013, **8**, e56894.